Polypropylene–Nanosilica-Filled Composites: Effects of Epoxy-Resin-Grafted Nanosilica on the Structural, Thermal, and Dynamic Mechanical Properties

Chaganti Srinivasa Reddy, Chapal Kumar Das

Materials Science Centre, Indian Institute of Technology, Kharagpur 721302, India

Received 9 August 2005; accepted 9 January 2006
DOI 10.1002/app.24131
Published online in Wiley InterScience (www.interscience.wiley.com).

ABSTRACT: This article reports a comparative study of polypropylene (PP) nanocomposites synthesized with nanosilica (NS) and diglycidyl ether of bisphenol A, an epoxy-resin-grafted nanosilica (ENS), as nanofillers. These nanocomposites were prepared with the melt-mixing method at a constant loading level of 2.5 wt %; this loading level was much lower than that used for fillers in conventional composites. The effects of pure NS and ENS on the thermal, structural, mechanical, and dynamic mechanical properties of PP were analyzed with wide-angle X-ray diffraction, transmission electron microscopy, thermogravimetric analysis, differential scanning calorimetry, dynamic mechanical analysis, and scanning electron microscopy. The transmission electron microscopy studies showed a better dispersion of ENS in the PP matrix, that is, in the polypropylene-epoxy-resin-grafted nanosilica (PP–ENS) nanocomposite, in comparison with NS in the PP matrix, that is, in the polypropylene–nanosilica (PP–NS) nanocomposite. Also, the thermogravimetric analysis results showed a higher thermal stability for PP–ENS than PP–NS. Furthermore, the dynamic mechanical analysis studies showed an increase in the elastic modulus and glass-transition temperature for PP–ENS with respect to PP–NS. J Appl Polym Sci 102: 2117–2124, 2006

Key words: fillers; fracture; glass transition; poly(propylene) (PP); thermal properties

INTRODUCTION

Polypropylene (PP) is a widely accepted choice in industries such as the packaging, automotive, and aviation industries and also finds substantial applications in household and other accessories. The reason that PP is such an obvious choice is the flexibility that it provides in terms of the modification of its structure and properties for various applications. One way of tailoring the properties of PP is the addition of appropriate fillers. In recent years, composites comprising PP and inorganic particulate fillers have achieved remarkable improvements in their mechanical and thermal properties with respect to pure PP. Also, nanometer-sized reinforcing particles have attracted considerable attention from polymer scientists. In particular, when compounding is performed to incorporate nanoparticles into a pure polymer matrix in such a way that the nanoscale particles are restricted to their ultrafine phase dimensions, the strong interfacial interactions of the polymer with these ultrafine nanoscale particles result in a significant improvement in the rigidity and strength of the final nanocomposite. In addition, the filler contents required for these nanoscale fillers are much lower in comparison with mineral- or glass-reinforced composites.[1]

Nanosilica (NS), with a large surface area, is widely used in polyolefin composites. Presently, the research on NS-based products is mainly focused on improving the mechanical and optical properties of polyolefins.[2–10]

The preparation of composite materials by the melt blending of polymers and fillers is a straightforward procedure, but it is less efficient when the reinforcing filler is in nanoscale. This is due to an agglomeration of nanoparticles along with the high melt viscosity of the polymers. To overcome these limitations in composite preparation, a first strategy based on filler encapsulation by polymer coating has been proposed.[11] Another approach relies on the chemical modification of the filler surface by functional silanes and titanate esters, which are able to promote adhesion to the polymer matrix.[12–17] However, the high cost of functional silane compounds also limits their usage for mass production.

As far as NS particles are concerned, three kinds of reactive hydroxyl groups—isolated, hydrogen-bonded, and geminated double-hydroxyl groups [sketched in Scheme 1(a)]—have been recently identified with IR

Correspondence to: C. K. Das (ckd@matsc.iitkgp.ernet.in).

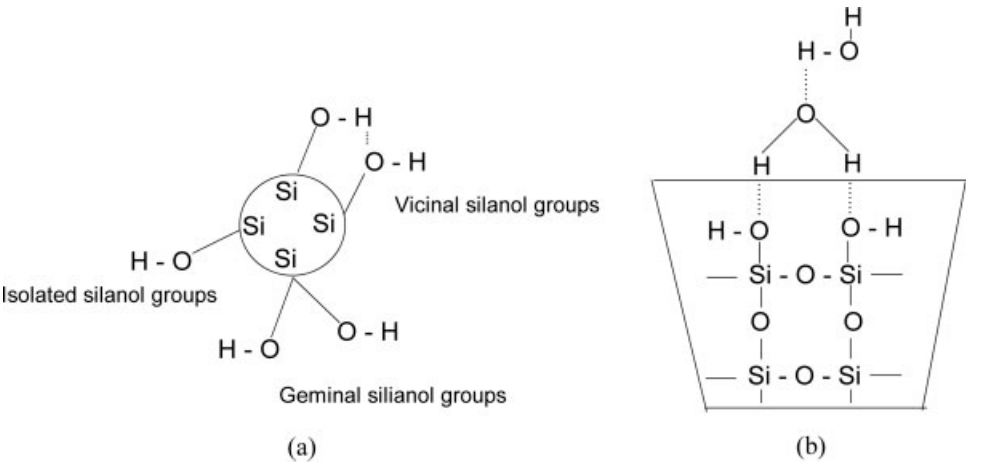

Scheme 1 (a) Types of surface silanol groups and (b) NS structure.

and NMR spectroscopy.[18] As shown in Scheme 1(b), synthetic NS is composed of four distinct layers. The first layer or inner core comprises random three-dimensional polymer SiO_2 units and is completely covered with silanol groups as the second layer. The third layer consists of water molecules, which are strongly bonded to the silanol groups. In the fourth layer, there is physically adsorbed water, also known as free water or free moisture.[19]

To improve the interfacial compatibility between the NS particles and PP, the hydrophilic surface of the NS particles was modified with epoxy resin with the reactive silanol groups of the NS particles. The melt-mixing technique was used to prepare the composite samples because it is an industrially viable method for mass production.

This work evaluates the various structural, thermal, and dynamic mechanical properties along with an analysis of the fracture nature of PP filled with NS and epoxy-resin-grafted nanosilica (ENS).

EXPERIMENTAL

Materials

Thermoplastic PP was obtained from IPCL (Vododara, India). NS was obtained from the Department of Chemistry of the Indian Institute of Technology (Kharagpur, India). The particle size was in the range of 50–60 nm, and the surface area was 360 m^2/g. It was prepared from an aqueous metal–silicate solution with the precipitation method.[10] The epoxy resin was liquid diglycidyl ether of bisphenol A (DGEBA; Araldite LY 556, Ciba–Geigy, India), which had an equivalent weight per epoxide group of 195 ± 5 and was used as received. Tin(II) chloride and methyl isobutyl ketone were obtained from Merck India, Ltd., and used as received.

Epoxy-resin grafting on NS

The reaction of silica particles with epoxy resin (DGEBA), a grafting agent, was carried out as follows.

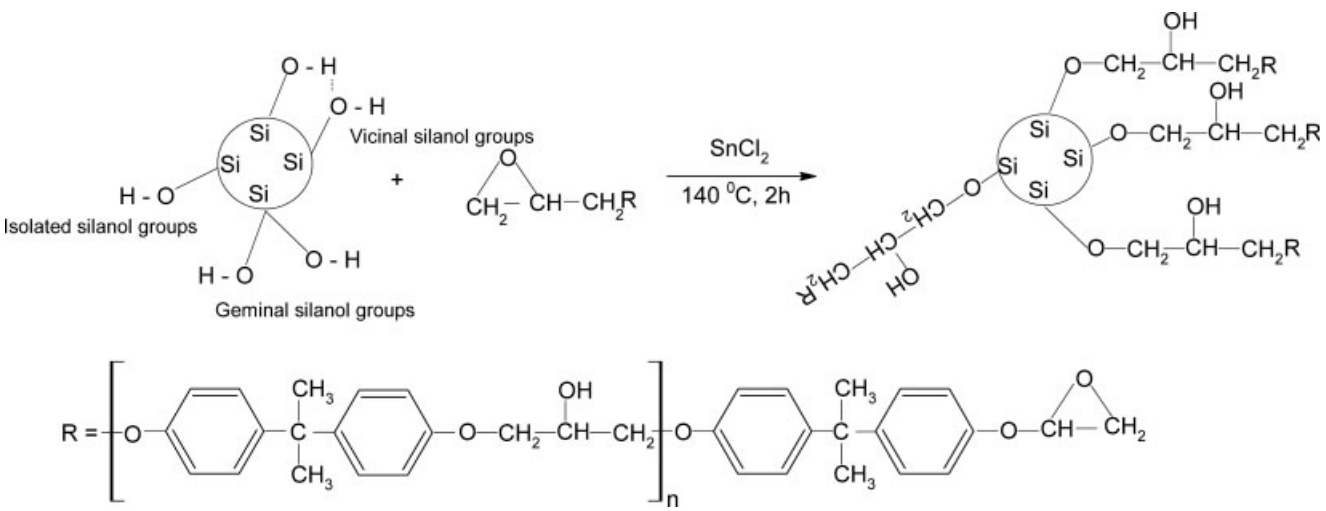

Scheme 2 Reaction mechanism of epoxy resin (DGEBA) grafting on NS.

TABLE I
Compounding Formulation of PP Nanocomposites

Sample configuration	Composition (wt %)		
	PP	NS	ENS
PP	100	0	0
PP–NS	100	2.5	0
PP–ENS	100	0	2.5

NS particles were first suspended in the solvent methyl isobutyl ketone. The epoxy resin was then added to the resulting NS particle suspension. The weight ratio of NS to the epoxy resin was taken to be 40 : 60. After the addition 1000 ppm $SnCl_2$ as a catalyst to the suspension, it was introduced into a three-necked, round-bottom flask equipped with a mechanical stirrer, a reflux condenser, and a thermometer. The reaction was carried out at 140°C for 2 h. After this, the solvent was removed with a rotary evaporator, and the product thus obtained was dried *in vacuo* for 1 h.

The reaction between the NS particles and oxirane groups of the epoxy resin has already been reported in our earlier work[10] (Scheme 2).

Preparation of the nanocomposites

Compounding PP with nanofillers was performed in the melt state in a corotating, twin-screw, sigma internal mixer at 200°C at a rotor speed of 100 rpm for 15 min. The formulations for the compounding are given in Table I. The blended composites thus obtained were drawn into sheets via compression molding at 200°C and a pressure of 15 MPa for 10 min. After this, the molded sheets were allowed to cool to room temperature under the same pressure at a rate of 2°C/min.

Methods and measurements

Wide-angle X-ray diffraction (WAXD)

This study was performed with a Philips PW 1840 X-ray diffractometer (Holland) with a copper target (Cu Kα) at a scanning rate of 0.050 2θ/s, at a chart speed of 10 mm/2θ, with a range of 5000 c/s, with a slit aperture of 0.2 mm, and with an operational voltage and current of 40 kV and 20 mA, respectively. This was done to assess the structural changes in PP in the presence of nanofillers.

Transmission electron microscopy (TEM)

A TEM study was performed with a Philips C 12 transmission electron microscope on very thin films of the composites cast directly over 300-mesh copper grids. The acceleration voltage was 120 kV, and the magnifications used for the images are given in the captions.

Mechanical properties

Dumbbell-shaped test samples were cut from molded sheets and were used for tensile testing at least 24 h after molding. Tensile tests were carried out with a Hounsfield HS 10 KS universal testing machine (Hounsfield Test Equipment Ltd., London) at room temperature with an extension speed of 5 mm/min and an initial gaze length of 35 mm. The reported results are the averages of four samples for each composite; each result had an experimental error of ±2%.

Thermogravimetry and differential scanning calorimetry (DSC) studies

The thermal stabilities of the composites were studied with a Dupont 2100 TGA V 50 1A thermogravimetric analyzer in the presence of air from 50 to 700°C, at a heating rate of 10°C/min. A DSC study was carried out in an inert atmosphere of nitrogen with a TA DSC Q1000 V7.0 differential scanning calorimeter. The data are reported for the second heating and first cooling runs from 60 to 200°C at 10°C/min.

Dynamic mechanical analysis (DMA)

DMA was carried out with a TA Instruments DMA-2980 dynamic mechanical analyzer (New Castle, Delaware, USA). The instrument was used in the single-cantilever bending mode. The samples were subjected to a sinusoidal displacement of 0.1% strain at a fixed frequency of 1 Hz from −30 to +150°C at a heating rate of 10°C/min. The storage modulus (E') and loss tangent (tan δ) were measured for each sample in this temperature range.

Scanning electron microscopy (SEM)

An SEM analysis was done with a JEOL JSM-5800 scanning electron microscope (Tokyo, Japan). This was

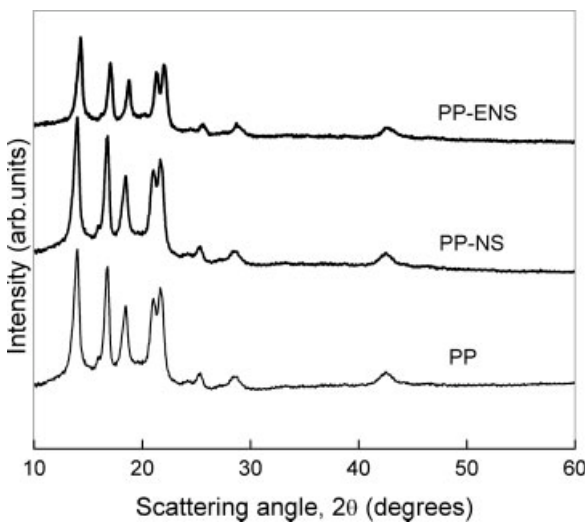

Figure 1 X-ray diffractograms of PP and its nanocomposites.

TABLE II
Results of the WAXD Study

Sample configuration	θ (°)				*d* (Å)				*L* (Å)			
	θ_1	θ_2	θ_3	θ_4	d_1	d_2	d_3	d_4	L_1	L_2	L_3	L_4
PP	14	16.8	18.5	21.7	6.33	5.28	4.80	4.10	185	235	186	72
PP–NS	14	16.8	18.4	21.6	6.33	5.28	4.81	4.12	187	243	191	72
PP–ENS	14.3	17.05	18.7	22.1	6.19	5.20	4.73	4.03	196	240	239	51

θ = peak angle; *d* = interplanar distance; *L* = crystallite size.

done to analyze the fracture nature of PP and the synthesized nanocomposites. For this, the fracture surfaces of the samples were first coated with gold by autosputtering.

RESULTS AND DISCUSSION

WAXD study

Figure 1 shows the X-ray diffractograms of PP, polypropylene–nanosilica (PP–NS), and polypropylene-epoxy-resin-grafted nanosilica (PP–ENS). Pure PP shows four prominent peaks at 2θ values of approximately 14, 16.8, 18.5, and 21.7°, each corresponding to the monoclinic α-crystalline phase of PP. New peaks do not appear with the addition of nanofillers to PP. However, the peaks at 2θ values of approximately 14 and 16.8° are slightly shifted to the higher angle side. These correspond to the 110_{PP} and 040_{PP} reflections of the α-crystalline phase, respectively. All the four earlier peaks are affected by the addition of nanofillers. However, this effect is more predominant in the case of PP filled with NS. The intensities of the four earlier peaks are reduced in the case of PP–NS. This is due to the absorption of X-ray radiation by the NS particles.[20] However, in the case of PP–ENS, the intensities of the four earlier peaks are further reduced. This decrease in the intensity suggests that PP–ENS attains lower crystallinity than PP–NS. The apparent crystallite size of the composites can be calculated with the Scherrer equation ($L = \lambda/(\beta \cos \theta)$, where *L* is the apparent crystal size, λ is the X-ray wavelength, and β is the full width at half-maximum of the peak. The diffraction angle, interplanar distance of the X-ray reflections, and crystallite size of PP and the synthesized nanocomposites are given in Table II. In the case of PP–ENS, the interplanar distance is reduced, and the crystallite size is increased. This decrease in the interplanar distance results in the development of a more compact structure in PP–ENS. Moreover, in the case of PP–ENS, there is a very genuine probability of the grafted epoxy-resin macromolecular chains occupy-

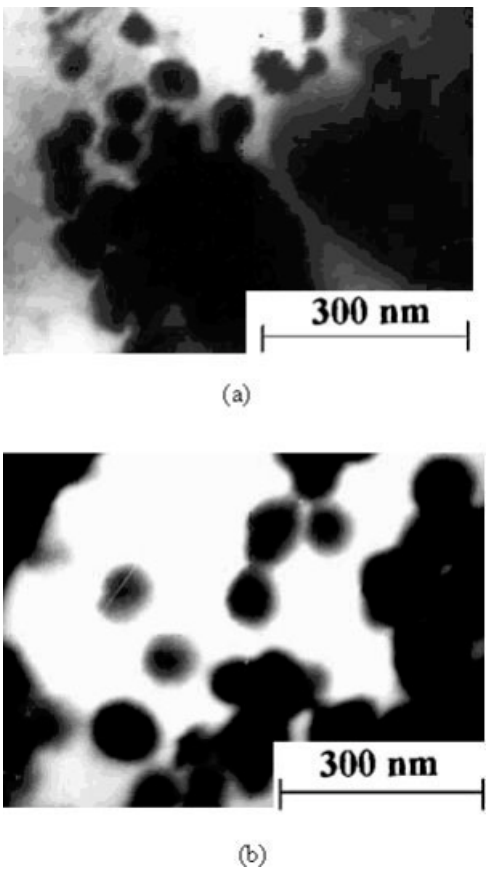

Figure 2 TEM micrographs of PP nanocomposites: (a) NS-filled PP (80,000×) and (b) ENS-filled PP (80,000×).

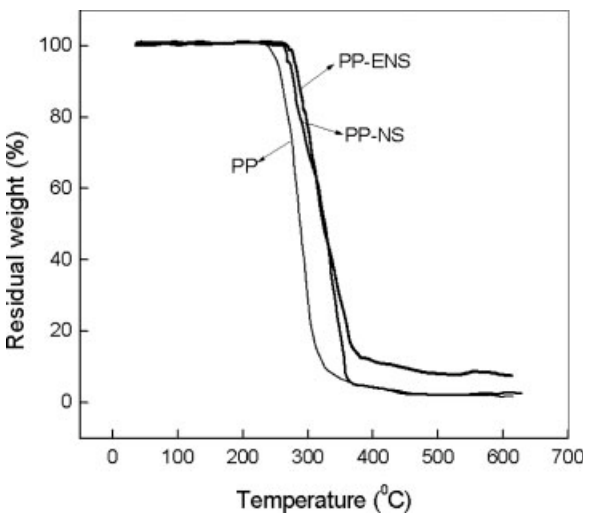

Figure 3 TGA thermograms of PP and its nanocomposites.

ing the chain-folded lamellar regions of PP. This may lead further to an expansion in the lamellar (crystallite) size of PP. This can be cited as a reason for the increase in the crystallite size of PP–ENS.

Morphological investigation

Figure 2(a,b) displays the respective TEM micrographs for PP–NS and PP–ENS. The micrograph for PP–NS shows the existence of black, spherical silica particles dispersed in the PP matrix in the form of chainlike structures consisting of NS agglomerates, which can be easily visualized from the micrograph. The micrograph for PP–ENS shows the individual silica particles; these are larger in size in comparison with NS. This is further supported by the fact that in the case of PP–ENS, there is a good dispersion of ENS in the PP matrix.

Thermal properties

Thermogravimetric analysis (TGA) was carried out for both nanocomposites and pure PP. The TGA curves are shown in Figure 3, and the corresponding parameters are listed in Table III. The decomposition temperature (temperature at 5% weight loss) is around 16°C higher for PP–NS (270°C) than that for PP (254°C). For PP–ENS, the decomposition temperature (282°C) is increased by 28°C with respect to that of pure PP. This suggests an improvement in the thermal stability for PP–ENS. This extent of the increase in the thermal stability may be due to the physical entanglements of the PP and epoxy-resin macromolecular chains of ENS. This could be the reason for the reduced rate of degradation for PP–ENS. These entanglements restrict the thermal motion of the PP chains. In fact, the degradation temperature for PP–ENS occurs at a higher temperature side with respect to PP–NS and pure PP. This implies that ENS significantly enhances the thermal stability of PP. Gilman[21] suggested that the high thermal stability of polymers in the presence of fillers is due to the hindered thermal motion of polymer molecular chains.

DSC curves of the nanocomposites and pure PP are shown in Figure 4(a,b), and the corresponding parameters are given in Table IV. The degree of crystallinity of the composites has been quantitatively measured with the following formula:

$$x = \frac{\Delta H_m}{\Delta H_0 \times \frac{m_p}{m_c}} \times 100$$

where x is the crystallinity percentage of the composite, ΔH_m is the melting enthalpy of PP, ΔH_0 is the melting enthalpy (209 J/g) of 100% crystalline PP,[22] m_p is the mass of PP, and m_c is the mass of the composite.

The melting temperature [Fig. 4 (a)] of PP remains the same in the presence of both kinds of nanofillers. The crystallization thermograms of the pure PP and the synthesized nanocomposites are shown in Figure 4(b). PP shows an exothermic crystallization peak at 115°C. A crystallinity of 42% has been calculated from the measurements of the melting enthalpy. PP–

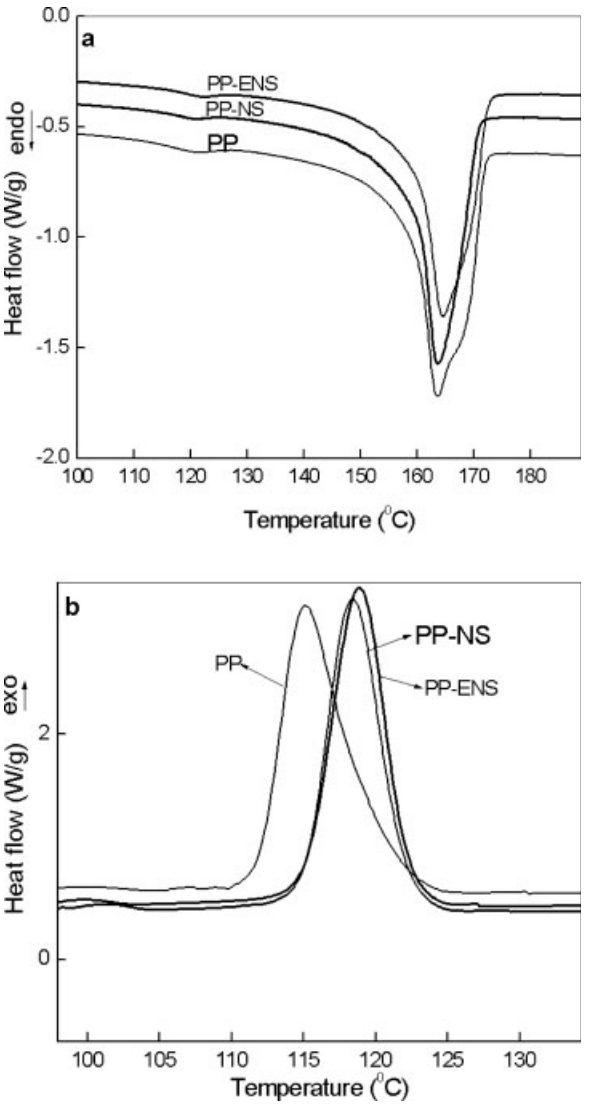

Figure 4 DSC thermograms of PP and its nanocomposites: (a) heating and (b) cooling.

TABLE III
Results of the TGA Study

Sample configuration	Temperature of 5% weight loss (°C)	Temperature of 10% weight loss (°C)	Temperature of 50% weight loss (°C)
PP	254	261	288
PP–NS	270	279	324
PP–ENS	282	286	327

TABLE IV
Results of the DSC Studies

Sample configuration	Melting temperature (°C)	Crystallization temperature (°C)	Supercooling temperature (°C)	Melting enthalpy (J/g)	Crystallization enthalpy (J/g)
PP	163	115	48	89	87
PP–NS	164	117	47	74	77
PP–ENS	163	118	45	64	80

NS shows a crystallization peak at 117°C with a corresponding crystallinity of 36%. In the case of PP–ENS, the crystallization point is increased to 118°C, with a corresponding crystallinity of 31%. The observed decrease in the crystallinity of the synthesized nanocomposites from the DSC measurements can be explained as follows. The adsorption of PP macromolecular chains on the surface of NS suggests polymer uncoiling and transformation from structures of higher energy to those of lower energy. However, this effect is more predominant for PP–ENS because of the formation of physical crosslinks between PP macromolecular chains and epoxy-resin macromolecular chains (from the surface of NS). The shift of the crystallization temperature toward the higher temperature side may be due to the nucleating capability of NS and ENS.

Tensile properties of the nanocomposites

The inclusion of fillers in the PP matrix leads to a significant increase in the modulus. Svehlova et al.[23] mentioned that a better filler dispersion leads to a higher modulus. This development can be explained by the percolation theory described by He and Jiang.[24] According to He and Jiang, there is a matrix zone around each particle, which is affected by the stress concentration. If the distance between particles is small enough, these zones join together and form a percolation network, which increases the modulus. For constant filler loadings, if the particles are fine and well dispersed, the total volume affect will be high, and the distance between the particles will be short. The percolation network, therefore, develops more easily, and the modulus increases. The stress–strain curves of PP and the synthesized nanocomposites are given in Figure 5, and the results are given in Table V.

In our composite system, the modulus of PP–NS is higher than that of PP, whereas PP–ENS has an intermediate modulus between those of PP and PP–NS. Also, the tensile strength and elongation at break decrease for PP–NS. This decrease in the tensile strength and elongation at break is due to the presence of NS agglomerates in the matrix as well as a lack of interfacial adhesion between the matrix and the filler (TEM images). However, in the case of PP–ENS, an increase in the tensile strength and elongation at break can be observed in comparison with those of PP and PP–NS. This may be because the epoxy-resin macromolecular chains grafted onto the NS surface have a tendency to obstruct the formation of agglomerates of the NS particles, thus allowing the NS particles to disperse in the matrix in the range of nanometer-scale clusters, which are smaller in size than NS clusters. The toughness of PP and the synthesized nanocomposites has been calculated by the measurement of the

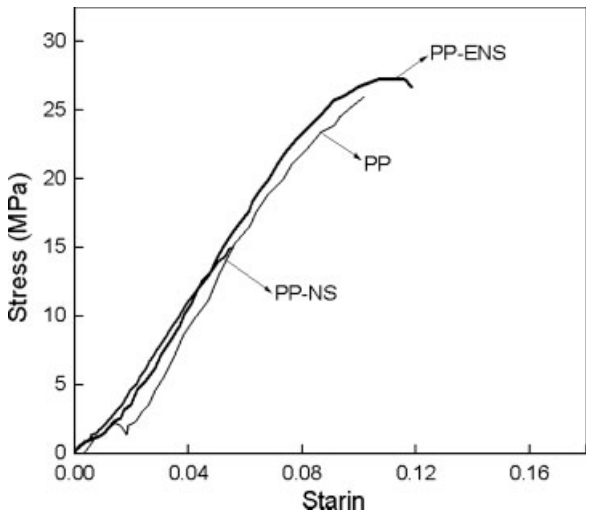

Figure 5 Stress–strain curves of the PP nanocomposites.

TABLE V
Results of the Tensile Test

Sample configuration	Tensile strength (MPa)	Elongation at break (%)	Elastic modulus (MPa)	Toughness (MJ/m^3)
PP	25.97	10	107.81	2.64
PP–NS	14.96	5	207.83	0.40
PP–ENS	27.28	11	198.62	2.95

TABLE VI
Dynamic Mechanical Properties of PP Nanocomposites

Sample configuration	T_g (°C)	Tan δ_{max}	E' at 25°C (GPa)
PP	18	0.14	7.23
PP–NS	18	0.11	8.91
PP–ENS	21	0.07	9.63

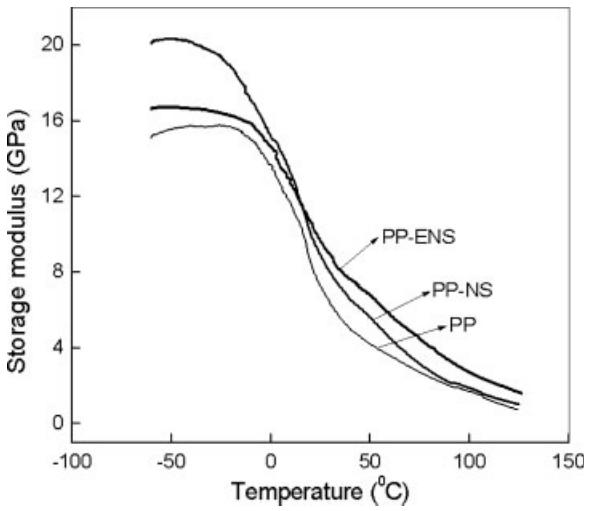

Figure 6 E' as a function of temperature of PP and its nanocomposites.

area under the stress–strain curves. The PP filled with NS shows a decrease in toughness, whereas PP filled with ENS shows a higher toughness with respect to PP. A similar observation was also reported by Rong et al.[25] for PP filled with polystyrene-grafted NS.

Dynamic mechanical properties

The dynamic mechanical properties of PP, PP filled with NS, and PP filled with ENS are presented in Table VI, and the results are compared with those of pure PP. The variations of E' and tan δ of PP and the synthesized nanocomposites against temperature are depicted in Figures 6 and 7. The glass-transition temperature (T_g) at the position of the maximum loss tangent (tan δ_{max} = 0.14) of pure PP is 18°C. The incorporation of NS causes a drop in tan δ_{max} to 0.11, whereas there is no noticeable change in T_g. However, for PP–NS, E' at room temperature is increased by 23%. A shift in T_g by +3°C, a drop in tan δ_{max} to 0.07, and an increase of E' at 25°C by 33% can be observed for ENS-filled PP.

E' always increases with the addition of NS fillers because NS is a stiffer material than PP. In the case of PP–NS, T_g of PP remains the same; this suggests there is not much interaction between NS and PP macromolecular chains. In the case of PP–ENS, T_g of PP is shifted toward a higher temperature side, sug-

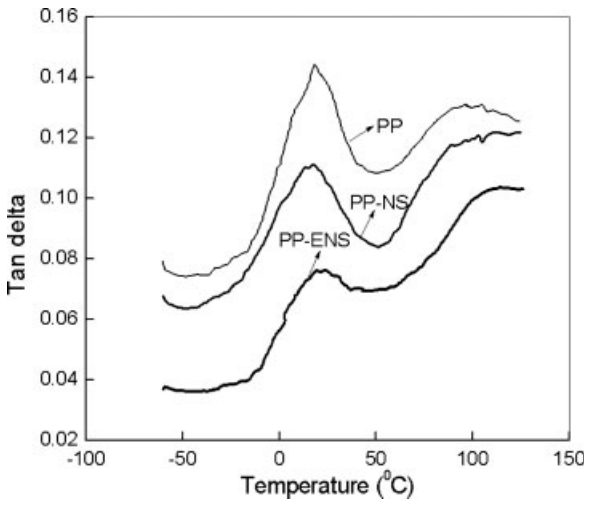

Figure 7 Tan δ as a function of temperature of PP and its nanocomposites.

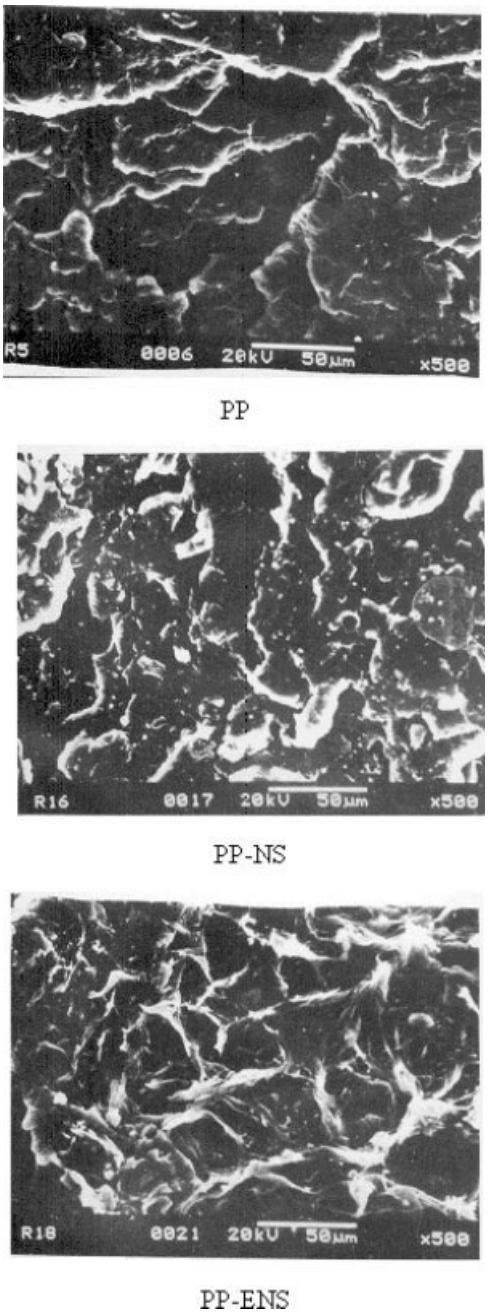

Figure 8 SEM tensile fracture surfaces of PP and its nanocomposites.

gesting the possible existence of interactions between ENS and PP macromolecular chains.

Fracture morphology

The SEM micrographs of the fractured surfaces obtained during the tensile testing of the nanocomposite specimens are shown in Figure 8. Pure PP has a smoother surface and exhibits no signs of plastic deformation or drawing. A coarser appearance can be observed for the fracture surface of PP–NS. However, we can still see a brittle type of failure in PP–NS. In contrast, PP filled with ENS shows clear evidence of moderate plastic deformation. This may be because the epoxy-resin-grafted macromolecular chains may also contribute to deformation.

CONCLUSIONS

The effects of NS and ENS on the structural, thermal, mechanical, and dynamic mechanical properties of PP have been studied. A TEM study has shown a good dispersion of silica particles in the case of PP–ENS. A DSC study has revealed that ENS has a greater influence in reducing the crystallinity of PP than NS. A TGA study has indicated that ENS has much more influence in increasing the thermal stability of PP with respect to NS. Tensile test results show that ENS provides PP with stiffening, strengthening, and toughening at a much lower loading level of 2.5 wt % with respect to NS. Also, a DMA study shows that T_g of PP increases in the presence of ENS. Finally, an SEM study suggests that PP–ENS shows moderate plastic deformation in comparison with pure PP and PP–NS.

References

1. Roy, R. Mater Sci Res 1986, 21, 25.
2. Sumita, M.; Ookuma, T.; Miyasaka, K. J Appl Polym Sci 1982, 27, 3059.
3. Sumita, M.; Tsukihi, T.; Miyasaka, K.; Ishikawa, K. J Appl Polym Sci 1984, 29, 1523.
4. Scott, C.; Ishida, H.; Maurer, F. H. J. J Mater Sci 1987, 22, 3936.
5. Scott, C.; Ishida, H.; Maurer, F. H. J. J Reinforced Plast Compos 1991, 10, 463.
6. Mizutani, Y.; Nago, S. J Appl Polym Sci 1999, 72, 1489.
7. Rong, M. Z.; Zhang, M. Q.; Zheng, Y. X. Polymer 2001, 42, 3301.
8. Wu, W.; Xu, Z. D. Acta Polym Sinica 2000, 1, 99.
9. He, P.; Zhao, A. C. Plastics 2001, 31, 39.
10. Reddy, C. S.; Das, C. K. Compos Interfaces 2005, 11, 687.
11. Hausslein, R. W.; Fallick, G. J Appl Polym Symp 1969, 11, 119.
12. Gahde, J. V.; Muller, V.; Lebedev, Y. V.; Lipatov, Y. S. Polym Sci USSR 1977, 19, 1446.
13. Solomon, D. H.; Rosser, M. J. J Appl Polym Sci 1965, 9, 1261.
14. Velasco-Santos, C.; Martinez-Hemandez, A. L.; Lozada-Cassou, M.; Alvarez-Castillo, A.; Castano, V. M. Nanotechnology 2002, 13, 495.
15. Carrot, G.; Rutot-Houze, D.; Pottier, A.; Degee, P.; Hilborn, J.; Dobois, P. Macromolecules 2002, 35, 8400.
16. Urzua-Sanchez, O.; Licea-Claverie, A.; Gonzalez, J.; Cota, L.; Castillon, F. Polym Bull 2002, 49, 39.
17. Lin, J.; Siddiqui, J. A.; Ottenbrite, R. M. Polym Adv Technol 2001, 12, 285.
18. Garoff, T. Presented at Techniques and Measurement in Heterogeneous and Homogeneous Catalysis, Liverpool, England, Sept 1993.
19. Katz, H. S.; Milewski, J. V. Handbook of Fillers for Plastics; Van Nostrand Reinhold: New York, 1987.
20. Reynaud, E.; Jouen, T.; Gauthier, C.; Vieger, G.; Varlet, J. Polymer 2001, 42, 8759.
21. Gilman, J. W. Appl Clay Sci 1999, 15, 31.
22. Marinelli, A. L.; Breatas, R. E. J Appl Polym Sci 2003, 87, 916.
23. Svehlova, V.; Polouek, E. Angew Makromol Chem 1994, 214, 91.
24. He, D.; Jiang, B. J Appl Polym Sci 1993, 49, 617.
25. Rong, M. Z.; Zhang, M. Q.; Zheng, Y. X.; Zeng, H. M.; Walter, R.; Friedrich, K. Polymer 2002, 42, 167.